Theoretical study of optimal synthesis conditions for superheavy element $Z = 119$*

Fang-Yu Chen (陈方宇)[1,2] Jia-Xing Li (李佳星)[1] Hong-Fei Zhang (张鸿飞)[1,3†]

[1]School of Physics, Xi'an Jiaotong University, Xi'an 710049, China
[2]School of Energy and Power Engineering, Xi'an Jiaotong University, Xi'an 710049, China
[3]School of Nuclear Science and Technology, Lanzhou University, Lanzhou 730000, China

Abstract: To optimize the reaction conditions for synthesizing the superheavy element $Z = 119$, we examined various combinations of projectiles and target nuclei used by different countries: Japan with $^{51}V + ^{248}Cm$, Russia potentially with $^{50}Ti + ^{249}Bk$, and China currently with $^{54}Cr + ^{243}Am$. Systematic investigations were conducted by varying the incident energy from 210 MeV to 260 MeV. We analyzed the capture cross sections, fusion probabilities, survival probabilities, and evaporation residue cross sections (ERCS) for each reaction to identify the optimal incident energy for synthesizing $Z = 119$. Detailed plots were generated for these parameters as functions of the incident energy, thereby providing valuable insights for selecting the most effective incident energy for synthesizing $Z = 119$.

Keywords: Superheavy nuclei, dinuclear system, incident energy, evaporation residue cross sections

DOI: 10.1088/1674-1137/adbe3e **CSTR:** 32044.14.ChinesePhysicsC.49064107

I. INTRODUCTION

Superheavy nuclei (SHN) synthesis is crucial in modern nuclear physics. First, it expands the known periodic table by creating new superheavy nuclei, which not only leads to the discovery of new chemical elements but also enhances our understanding of element periodicity and nuclear stability. This research addresses fundamental questions regarding the limits of mass and charge in atomic nuclei. By examining the decay properties and stability of superheavy elements, researchers can infer the potential limits of the atomic nucleus and explore their behavior under extreme conditions [1, 2]. Additionally, SHN research provides valuable experimental data to test and refine nuclear structure theories, including the shell model, relativistic mean-field theory, and macroscopic-microscopic models. These models are crucial for predicting the locations of "magic numbers" and region of the "island of stability" [3, 4]. By synthesizing the nuclei near the predicted "island of stability", scientists investigate shell effects, where certain superheavy nuclei exhibit increased stability than others, thereby providing insights into nuclear stability mechanisms. Further, SHN investigations pushes the boundaries of nuclear physics, advancing research on nuclear reactions and structures under extreme conditions. This not only broadens our knowledge of the microscopic world but also fosters the development of nuclear experimental techniques and theoretical computational methods. While most synthesized superheavy nuclei are currently unstable, their synthesis may reveal new physical phenomena or potential applications, notably in fields of nuclear energy, medicine, and materials science.

The central issue in SHN research is determining the location of the "island of stability" and understanding the structure and decay properties of the nuclei in this region, particularly how to effectively synthesize these superheavy elements. Several theoretical approaches have been developed to address these issues, including the two-step model [5], macroscopic dynamics model [6, 7], multidimensional Langevin-type dynamical equations [8−12], time-dependent Hartree-Fock theory (TDHF) [13], extension time-dependent density-matrix theory (TDDM) [14], and dinuclear system (DNS) model [15−22]. These models predict varying locations for the island of stability. Proton numbers primarily include $Z = 114$, 120, and 126, while neutron numbers include $N = 176$, 184, 196, and 228 [23, 24]. Almost all models predict $N = 184$ as a neutron magic number. So far, all the synthesized superheavy nuclei lie on the proton-rich side. For element 114, seven isotopes have been synthesized, with the highest neutron number reaching $N = 176$, leaving eight neutrons short of the magic number $N = 184$. With the development of heavy ion accelerators and related detection equipment, the synthesis of element 119 [25−27] is cur-

Received 4 October 2024; Accepted 7 March 2025; Published online 8 March 2025
* Supported by the National Natural Science Foundation of China (12175170, 11675066)
† E-mail: zhanghongfei@lzu.edu.cn

rently on the agenda following the synthesis of element $Z = 118$ [28, 29], which completed the seventh row of the periodic table.

Synthesizing new elements 119 and 120 is crucial, as it advances the exploration of mass and charge limits of superheavy nuclei, brings us closer to synthesizing nuclei with neutron numbers approaching 184, and synthesizes nuclei near the proton magic number $Z = 120$. Thus, the synthesis of these elements is crucial in nuclear physics. Major nuclear physics laboratories worldwide, including those in the U.S., Russia, Germany, Japan, and China, are competing to synthesize element 119. Japan is conducting experiments using the $^{51}\mathrm{V}+^{248}\mathrm{Cm}$ reaction, while Russia is expected to use the $^{50}\mathrm{Ti}+^{249}\mathrm{Bk}$ reaction, and China is focusing on the $^{54}\mathrm{Cr}+^{243}\mathrm{Am}$ reaction. These laboratories have identified three key projectile-target combinations for experimental investigations. A primary theoretical challenge in investigating these combinations for synthesizing element 119 includes predicting the optimal incident energy and evaporation residue cross-section. Determining the optimal incident energy is crucial for the successful production of superheavy nuclei, while the theoretically predicted evaporation residue cross-section facilitate their experimental identification. Thus, this theoretical study aims to provide insights for the ongoing experiments.

II. THEORETICAL FRAMEWORK

In the DNS model, SHN is divided into three key stages: capture, fusion, and survival. Initially, two nuclei must overcome the Coulomb barrier to form a dinuclear system, which is represented by the capture cross-section. In the next step, the dinuclear system may either fuse into a compound nucleus or undergo quasifission, a competition described by the fusion cross-section. Finally, the excited compound nucleus de-excites by emitting neutrons while competing with fission. The survival probability of this compound nucleus is determined using a statistical model. In the DNS approach, ERCS is expressed as follows [30−33]:

$$\sigma_{\mathrm{ER}}(E_{\mathrm{c.m.}}) = \frac{\pi\hbar^2}{2\mu E_{\mathrm{c.m.}}}\sum_J (2J+1) \times T(E_{\mathrm{c.m.}},J)P_{\mathrm{CN}}(E_{\mathrm{c.m.}},J)W_{\mathrm{sur}}(E_{\mathrm{c.m.}},J), \quad (1)$$

where $E_{\mathrm{c.m.}}$ represents the incident energy in the center-of-mass frame, J the orbital angular momentum of the relative motion, and $T(E_{\mathrm{c.m.}},J)$ the transmission probability, which determines the likelihood of the colliding nuclei overcoming the potential barrier to form the dinuclear system. $P_{\mathrm{CN}}(E_{\mathrm{c.m.}},J)$ represents the probability of the system proceeding to form a compound nucleus and $W_{\mathrm{sur}}(E_{\mathrm{c.m.}},J)$ the survival probability of the compound nucleus after its excitation [34].

A. Capture cross section

For heavy-ion fusion reactions, the transmission probability $T(E_{\mathrm{c.m.}},J)$ is often calculated using the Hill-Wheeler formula as follows [35]:

$$T(E_{\mathrm{c.m.}},J) = \frac{1}{1+\exp\left(-\frac{2\pi}{\hbar\omega(J)}\left[E_{\mathrm{c.m.}}-V_B-\frac{\hbar^2}{2\mu R_V^2}J(J+1)\right]\right)}. \quad (2)$$

In this context, V_B, $R_V(J)$, and $\hbar\omega(J) = \sqrt{\frac{\hbar^2}{\mu}\left|\frac{\partial^2 V}{\partial r^2}\right|_{V_B}}$ represent the height, position, and curvature of the barrier, respectively. As the projectile and target nuclei approach each other, dynamic deformation may occur. The distribution of the interaction potential barrier between the interacting projectile and target nuclei is primarily caused by the dynamic deformation of the nuclei. Consequently, the interaction potential between the projectile and target nuclei can be expressed as the sum of the Coulomb potential, nuclear potential, and deformation energy potential as follows [36]:

$$V(r,\beta_p,\beta_t,\theta_1,\theta_2) = V_C(r,\beta_p,\beta_t,\theta_1,\theta_2)+V_N(r,\beta_p,\beta_t,\theta_1,\theta_2) + \frac{1}{2}C_1(\beta_p-\beta_p^0)^2+\frac{1}{2}C_2(\beta_t-\beta_t^0)^2, \quad (3)$$

where θ_1 and θ_2 represent the angles between the radius vector r and symmetry axes of the projectile and target nuclei, respectively. β_p^0 and β_t^0 represent the static deformation coefficients of the projectile and target nuclei, respectively, and are usually taken as the quadrupole deformation parameters of the nuclei. In this study, the quadrupole deformation parameters of the ground state for the reacting nuclei are obtained from reference [37] (see Table 1). β_p andβ_t represent their dynamic deformation coefficients. It is assumed that the deformation energy is proportional to the mass number: $\frac{C_1\beta_p^2}{C_2\beta_t^2} = \frac{A_p}{A_t}$ [9].The constants C_1 and C_2 represent the nuclear surface stiffness parameters of the projectile and target nucleus calculated using the liquid drop model, respectively [38].

$$C_i = (\lambda-1)\left[(\lambda+2)R_{0,i}^2\sigma-\frac{3}{2\pi}\frac{Z_i^2e^2}{R_{0,i}(2\lambda+1)}\right], \quad (4)$$

where λ represents the mode of the dynamic deformation. In this case, only quadrupole deformation ($\lambda = 2$) is considered. R_0 represents the radius in the spherical case. The surface tension parameter σ is related to the surface

Table 1. Quadrupole deformation parameter β_2 of the ground states of the nuclei used in the calculations for this study[37].

Nucleus	^{51}V	^{248}Cm	^{50}Ti	^{249}Bk	^{54}Cr	^{243}Am
β_2	0.021	0.250	0.000	0.250	0.161	0.237

[a] Note: All nuclear masses used in this study are taken from Ref. [37].

energy by $4\pi R_0^2\sigma = a_s A^{2/3}$, with $a_s = 18.32$ MeV. The Coulomb potential is expressed as follows [39]:

$$\begin{aligned} V_C(r,\beta_p,\beta_t,\theta_1,\theta_2) = &\frac{Z_1Z_2e^2}{r} \\ &+\sqrt{\frac{9}{20\pi}}\frac{Z_1Z_2e^2}{r^3}\sum_{i=1}^{2}R_i^2\beta_iP_2(\cos\theta_i) \\ &+\frac{3}{7\pi}\frac{Z_1Z_2e^2}{r^3}\sum_{i=1}^{2}R_i^2\left[\beta_iP_2(\cos\theta_i)\right]^2. \end{aligned} \quad (5)$$

The nuclear potential can be written as follows [40]:

$$\begin{aligned} V_N(r,\beta_p,\beta_t,\theta_1,\theta_2) = &-V_0 \\ &\times\left\{1+\exp\left[\frac{r-\sum_{i=1}^{2}R_i\left(1+\sqrt{\frac{5}{4\pi}}\beta_iP_2(\cos\theta_i)\right)}{a}\right]\right\}^{-1} \end{aligned} \quad (6)$$

where θ_i represents the angle between the symmetry axis of the i-th nucleus and direction of collision, R_i the radius of the i-th nucleus, and parameter β_i the deformation of the projectile and target nuclei.

Considering the channel coupling effect through the potential barrier distribution, the transmission probability is expressed as follows [41]:

$$T(E_{\rm c.m.},J) = \int f(V_B)T(E_{\rm c.m.},J)\mathrm{d}V_B, \quad (7)$$

where $f(V_B)$ represents an asymmetric Gaussian function

$$f(V_B) = \begin{cases} \frac{1}{N}\exp\left[-\left(\frac{V_B-V_m}{\Delta_1}\right)^2\right], & \text{for } V_B < V_m, \\ \frac{1}{N}\exp\left[-\left(\frac{V_B-V_m}{\Delta_2}\right)^2\right], & \text{for } V_B > V_m. \end{cases} \quad (8)$$

In the equation, the distribution width is expressed as $\Delta_2 = (V_0 - V_s)/2$, while $\Delta_1 = \Delta_2 - 2\,\mathrm{MeV}$. $V_m = (V_0 + V_s)/2$, where V_0 and V_s represent the Coulomb barrier height at the waist-to-waist collision and barrier height at the deformation saddle point (the point of minimum deformation), respectively. N represents the normalization constant, which is expressed as $\int f(B)\mathrm{d}B = 1$.

B. Complete fusion probability

To calculate the fusion probability in the DNS model, the fusion process is treated as a diffusion phenomenon by solving a set of master equations over the potential energy surface (PES). At any given time t, the probability of finding a dinuclear configuration (Z_1,N_1), where Z_1 represents the number of protons and N_1 the number of neutrons corresponding to a given configuration, is denoted by $P(Z_1,N_1,t)$. The time evolution of this distribution probability $P(Z_1,N_1,t)$ can be described using a two-dimensional master equation with the number of protons and neutrons as variables [42].

$$\begin{aligned} \frac{\mathrm{d}P(Z_1,N_1,E_1,t)}{\mathrm{d}t} = &\sum_{Z_1'}W_{Z_1,N_1;Z_1',N_1}(t)\left[d_{Z_1,N_1}P(Z_1',N_1,E_1',t)\right] \\ &-\sum_{Z_1'}W_{Z_1,N_1;Z_1',N_1}(t)\left[d_{Z_1',N_1}P(Z_1,N_1,E_1,t)\right] \\ &+\sum_{N_1'}W_{Z_1,N_1;Z_1,N_1'}(t)\left[d_{Z_1,N_1}P(Z_1,N_1',E_1',t)\right] \\ &-\sum_{N_1'}W_{Z_1,N_1;Z_1,N_1'}(t)\left[d_{Z_1,N_1'}P(Z_1,N_1,E_1,t)\right] \\ &-\left\{q_f[\epsilon(t)]\right\}P(Z_1,N_1,E_1,t) \\ &-\{f_s[\epsilon(t)]\}P(Z_1,N_1,E_1,t). \end{aligned} \quad (9)$$

where $W_{Z_1,N_1;Z_1',N_1}$ represents the mean transition probability between channels (Z_1,N_1) and (Z_1',N_1), and d_{Z_1,N_1} the microscopic dimension associated with the macroscopic state (Z_1,N_1). The evolution of the DNS model along the internuclear distance R can lead to quasifission, which is quantified by the quasifission rate q_f. The fission rate f_s, estimated using the Kramers formula, corresponds with the local excitation energy E_1 of a specific dinuclear configuration, with the detailed formula expressed by Equation (19).

If the transitions between different configurations of a dinuclear system only consider energy transitions and nucleon transfers, then the transition probability for the neutron transfer can be expressed as follows [43]:

$$\begin{aligned} W_{Z_1,N_1;Z_1,N_1'}(t) = &\frac{\tau_{\rm mem}(Z_1,N_1,E_1,N_1',E_1';t)}{\hbar^2 d_{Z_1,N_1}d_{Z_1,N_1'}} \\ &\times\sum_{ii'}\left|\langle Z_1,N_1',E_1',i'|V|Z_1,N_1,E_1,i\rangle\right|^2, \end{aligned} \quad (10)$$

where i denotes other quantum numbers.

To simplify the numerical solution of the main equation, it is assumed that in the nucleon transfer process, only single nucleon transitions are dominant, while double or multi-nucleon simultaneous transitions are neglected. The transition probability $W_{N_1,Z_1;N_1',Z_1}$ between different states of the dinuclear system only occurs when $N_1' = N_1 \pm 1$ (or $Z_1' = Z_1 \pm 1$). When considering only the transfer of one neutron, the above equation can be written as follows [44]:

$$\begin{aligned} & W_{Z_1,N_1;Z_1,N_1'}(t) \\ = & \frac{\tau_{\rm mem}(Z_1,N_1,E_1,N_1',E_1';t)}{\hbar^2 d_{Z_1,N_1} d_{Z_1,N_1'}} \\ & \times \left\{ \left[\omega_{11}(Z_1,N_1,E_1,E_1') + \omega_{22}(Z_1,N_1,E_1,E_1') \right] \delta_{N',N} \right. \\ & + \omega_{12}(Z_1,N_1,E_1,E_1')\delta_{N',N-1} \\ & \left. + \omega_{21}(Z_1,N_1,E_1,E_1')\delta_{N',N+1} \right\}. \end{aligned} \tag{11}$$

The memory time is expressed as

$$\tau_{\rm mem}(Z_1,N_1,E_1,N_1',E_1';t) = \hbar \left[\frac{2\pi}{\sum_{KK'} \langle V_{KK'} V_{KK'}^* \rangle} \right]^{1/2}, \tag{12}$$

$$\omega_{KK'}(Z_1,N_1,E_1,E_1') = d_{Z_1,N_1} \langle V_{KK'} V_{KK'}^* \rangle, \tag{13}$$

$$\begin{aligned} \langle V_{KK'} V_{KK'}^* \rangle = & \frac{1}{4} U_{KK'}^2 g_K g_{K'} \Delta_{KK'} \cdot \Delta\varepsilon_K \cdot \Delta\varepsilon_{K'} \\ & \times \left[\Delta_{KK'}^2 + \frac{1}{6} \left(\Delta\varepsilon_K^2 + \Delta\varepsilon_{K'}^2 \right) \right]. \end{aligned} \tag{14}$$

The interaction strength factor is expressed as

$$U_{KK'} = \frac{g_1^{1/3} g_2^{1/3}}{g_1^{1/3} + g_2^{1/3}} \frac{1}{g_K^{1/3} g_{K'}^{1/3}} \cdot 2\gamma_{KK'}. \tag{15}$$

The factor $\gamma_{KK'}$ represents the reduced interaction strength and $\Delta_{KK'}$ the width of the interaction strength distribution. In practical calculations, both are taken as constants: $\gamma_{KK'} = 3$ and $\Delta_{KK'} = 2$ $(K, K' = 1, 2)$. $\Delta\varepsilon_K$ represents the valence space and is expressed as $\Delta\varepsilon_K = \Delta\varepsilon = \sqrt{4\varepsilon/g}$ [45], where $\varepsilon \equiv \varepsilon(Z_1, N_1)$ represents the local excitation energy corresponding to the dinuclear configuration (Z_1, N_1). For the proton transfer process, the aforementioned approach can be applied.

In the nucleon transfer process, the dinuclear system is influenced by the PES, which forms the mass distribution probability which evolves over time. The potential energy surface is expressed as follows [46]:

$$\begin{aligned} V(N_1,Z_1;N_2,Z_2,R,\beta_a,\beta_b,J) = & B(Z_1,N_1,\beta_a) \\ & + B(Z_2,N_2,\beta_b) - \left[B(Z,N,\beta) + V_{\rm rot}^{\rm CN}(J) \right] \\ & + V(N_1,Z_1;N_2,Z_2,J,R;\beta_a,\beta_b), \end{aligned} \tag{16}$$

where $N = N_1 + N_2$ and $Z = Z_1 + Z_2$, with β, β_a, and β_b representing the quadrupole deformation parameters of the compound nucleus and two deformed nuclei, respectively. The binding energies of the compound nucleus and two deformed nuclei, denoted as $B(Z,N,\beta)$, $B(Z_1,N_1,\beta_a)$, and $B(Z_2,N_2,\beta_b)$, are sourced from reference [37]. $V_{\rm rot}^{\rm CN}(J)$ represents the rotational energy of the compound nucleus. The interaction potential between the two deformed nuclei includes the nuclear, Coulomb, and centrifugal potentials.

$$\begin{aligned} V(N_1,Z_1;N_2,Z_2,J,R;\beta_a,\beta_b) = & V_{\rm C}(Z_1,Z_2,\beta_a,\beta_b,R) \\ & + V_N(N_1,Z_1,N_2,Z_2,\beta_a,\beta_b,J) + \frac{J(J+1)\hbar^2}{2\mu R^2}. \end{aligned} \tag{17}$$

The reduced mass μ is expressed as

$$\mu = \frac{m \cdot A_1 A_2}{A_1 + A_2}, \tag{18}$$

where m represents the nucleon mass, and A_1 and A_2 the masses of the two fragments. $V_{\rm C}$ represents the Coulomb potential and V_N the nuclear interaction potential.

In a dinuclear system, the local excitation energy corresponding to a specific dinuclear configuration (Z_1, N_1) is determined by the dissipation of the relative kinetic energy between the projectile and target nuclei into the dissipated energy of the dinuclear system, along with the driving potential of the system. This relationship can be expressed as follows [36]:

$$\begin{aligned} \varepsilon^*(t) = & E_{\rm dis}(t) - (V(Z_1,N_1) - V(Z_P,N_P)) \\ & - \frac{(J-M)^2}{2\Im_{\rm rel}} - \frac{M^2}{2\Im_{\rm int}}, \end{aligned} \tag{19}$$

where $E_{\rm dis}(t)$ represents the dissipated energy transferred from the relative motion between the projectile and target nuclei into the dinuclear system (see Equation (25)), varying with the interaction time. J and M represent the initial relative orbital angular momentum of the incident channel and dissipated angular momentum that becomes the intrinsic angular momentum of the dinuclear system, respectively. $V(Z_1,N_1)$ denotes the potential energy corresponding to a particular dinuclear configuration (Z_1,N_1) within the dinuclear system, while $V(Z_P,N_P)$ the potential energy of the dinuclear system at the entrance point. The local excitation energy of the dinuclear system is re-

lated to its driving potential. $\Im_{\rm rel}$ and $\Im_{\rm int}$ represent the moment of inertia for the relative motion in the entrance channel and intrinsic moment of inertia of the dinuclear system, respectively, expressed as follows [44]:

$$\Im_{\rm rel} = \mu R^2, \tag{20}$$

$$\Im_{\rm int} = \frac{2}{5}\left(m_1 R_1^2 + m_2 R_2^2\right), \tag{21}$$

where R_1 and R_2 represent the radii of the projectile and target nuclei, respectively, and m_1 and m_2 the masses of the projectile and target nuclei, respectively.

Under the combined influence of the Coulomb and nuclear force, atomic nuclei can undergo deformation. Assuming that the deformation of the fragments evolves in an overdamped motion, the relative distance between the centers of the fragments $r(t)$ is expressed as follows [47, 48]:

$$\begin{aligned} r(t) &= (R_1 + R_2)[1 + a(t)] \\ a(t) &= a_0\left[1 - \exp\left(-\frac{t}{\tau_{\rm def}}\right)\right]. \end{aligned} \tag{22}$$

The maximum dynamic deformation a_0 can be obtained by minimizing the interaction potential energy between the projectile and target nuclei, with $\tau_{\rm def}$ representing the deformation relaxation time, generally approximated as 5×10^{-21} s.

The relative kinetic energy and angular momentum of the projectile and target nuclei are dissipated and transformed into the intrinsic excitation energy and angular momentum of the compound system. The dissipative behavior of the relative radial kinetic energy in the incident channel over time is expressed using the Fokker-Planck equation. The average radial kinetic energy is expressed as follows [44]:

$$E_{\rm rad}(t) = E_i \exp\left(-\frac{t}{\tau_{\rm rad}}\right), \tag{23}$$

where E_i represents the initial radial kinetic energy and $\tau_{\rm rad}$ the relaxation time of the radial motion (expressed 5×10^{-22} s).

The final state energy is related to the following expression [44]:

$$E_f(t) = \frac{Z_1 Z_2 e^2}{r(t)} + \frac{\hbar^2 l^2(t)}{2\Im_{\rm rel}(t)} + E_{\rm rad}(t), \tag{24}$$

where $l(t)$ represents the angular momentum, which is time-dependent.

According to the principle of energy conservation, the relative kinetic energy between the projectile and target nuclei is converted into the excitation energy of the system. The corresponding dissipated energy can be expressed as follows:

$$E_{\rm dis}(t) = E_{\rm c.m.} - E_f(t). \tag{25}$$

The probability of the compound nucleus formation, considering the Coulomb barrier V_B, is expressed as follows [49]:

$$P_{\rm CN}(E_{\rm c.m.}, J, V_B) = \sum_{Z_1=1}^{Z_{\rm BG}} \sum_{N_1=1}^{N_{\rm BG}} P(Z_1, N_1, E_1, \tau_{\rm int}), \tag{26}$$

where $Z_{\rm BG}$ and $N_{\rm BG}$ represent the charge and neutron numbers at the Businaro-Gallone (BG) point, and $\tau_{\rm int}$ the interaction time, which depends on the center-of-mass energy $E_{\rm c.m.}$, angular momentum J, and barrier V_B. The overall fusion probability is expressed as follows:

$$P_{\rm CN}(E_{\rm c.m.}, J) = \int f(V_B) P_{\rm CN}(E_{\rm c.m.}, J, V_B) {\rm d}V_B. \tag{27}$$

C. Survival probability

Once the compound nucleus is formed, it de-excites by evaporating neutrons or emitting gamma radiation, with fission being an alternative process. The probability of the compound nucleus surviving by evaporating x neutrons is expressed as follows:

$$W_{\rm sur}(E^*_{\rm CN}, x, J) = P(E^*_{\rm CN}, x, J) \prod_{i=1}^{x} \frac{\Gamma_n(E_i^*, J)}{\Gamma_n(E_i^*, J) + \Gamma_f(E_i^*, J)}, \tag{28}$$

where $E^*_{\rm CN} = E_{\rm c.m.} + Q$ represents the excitation energy of the compound nucleus, E_i^* the excitation energy before the i-th neutron is evaporated, and $\Gamma_n(E_i^*, J)$ and $\Gamma_f(E_i^*, J)$ the partial decay widths for neutron emission and fission, respectively [36].

III. RESULTS AND DISCUSSIONS

To determine the optimal incident energy for synthesizing element 119, we used the DNS model to analyze the reaction ^{51}V + ^{248}Cm (Japan), ^{50}Ti + ^{249}Bk (Russia), and ^{54}Cr + ^{243}Am (China). We systematically varied the incident energy and analyzed the capture cross section, fusion probability, survival probability, and ERCS.

As shown in Fig. 1, the capture cross section for the ^{50}Ti + ^{249}Bk reaction is higher than that for the ^{51}V + ^{248}Cm and ^{54}Cr + ^{243}Am combinations owing to the combined effects of the Coulomb barrier, nuclear potential barrier,

and incident energy. The Coulomb barrier is determined by the number of protons in the nuclei, with more protons leading to stronger Coulomb repulsion and a higher barrier. Since ^{50}Ti has fewer protons, the Coulomb barrier for its combination with ^{249}Bk is lower, making it easier to overcome the barrier and reach an effective distance to the target nucleus at lower incident energies. Additionally, the nuclear potential barrier is influenced by nuclear deformation.^{249}Bk exhibits significant deformation, which reduces the nuclear potential barrier during the collision process and allows for effective capture and compound nucleus formation at lower energies. Further, the incident energy is crucial in determining the efficiency of compound nucleus formation. For the ^{50}Ti+^{249}Bk combination, the lower Coulomb and nuclear barriers facilitate formation of the compound nucleus a similar incident energy, thereby resulting in a rapid increase in the capture cross section. These factors contribute to the higher capture cross section of ^{50}Ti+^{249}Bk across the entire energy range than the other two combinations. As shown in the comparison of capture cross sections for different reactions, where the ^{50}Ti+^{249}Bk combination has a significantly higher capture cross section than the others, indicating that this combination can effectively form a compound nucleus even at lower incident energies.

Figure 2 shows the relationship between the fusion probability and excitation energy for the three reactions. At similar excitation energies, the fusion probabilities of ^{51}V+^{248}Cm and ^{50}Ti+^{249}Bk are similar and higher than that of ^{54}Cr+^{243}Am. This is because the total number of protons and neutrons in the dinuclear systems of the first two reactions is similar, while in the third reaction, the fusion probability is lower owing to the smaller mass asymmetry.

As shown in Fig. 3, the survival probabilities of the different compound nuclei are compared, highlighting the lower survival probability of the nucleus formed from ^{54}Cr+^{243}Am. The survival probability of the compound nucleus formed from the ^{54}Cr+^{243}Am combination is slightly lower than that of the other two, primarily because the compound nucleus has two fewer neutrons. This decrease in the neutron number directly impacts the stability of the nucleus. Neutrons are crucial in the stability of nuclei, notably in the synthesis of superheavy elements, where an appropriate neutron-to-proton ratio is key to counteract the strong repulsive forces between protons. A deficiency in neutrons can reduce the stability of the compound nucleus, making it more prone to fission or other radioactive decay processes. Additionally, nuclei with fewer neutrons generally have lower binding energies, leading to shorter half-lives and reduced survival probability. Therefore, the lower neutron number in the compound nucleus formed from the ^{54}Cr+^{243}Am results in relatively lower stability and shorter survival time in experimental settings.

As shown in Fig. 4, the cross sections for the production of element 119 are plotted against the incident energy for the various reaction pathways of the three reactions. To determine the optimal incident energy and reaction path for achieving the maximum probability of synthesizing element 119, the highest point on each curve must be identified. These peaks represent the optimal in-

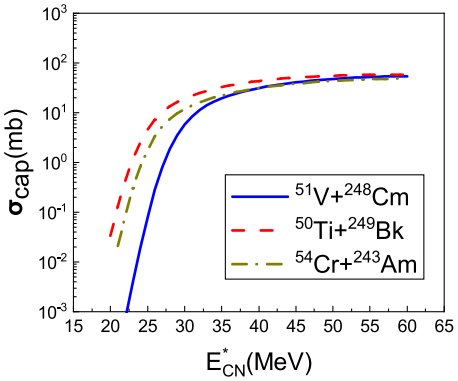

Fig. 1. (color online) Calculated capture cross sections as a function of the excitation energy for the three reactions.

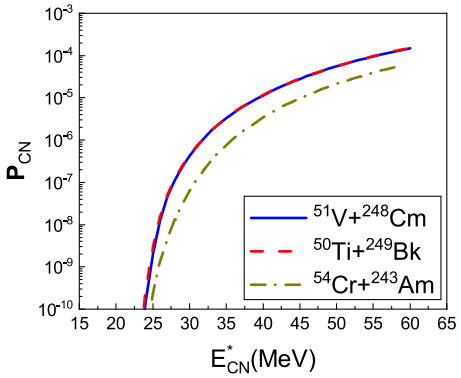

Fig. 2. (color online) Calculated fusion probability curves as a function of the excitation energy for the three reactions.

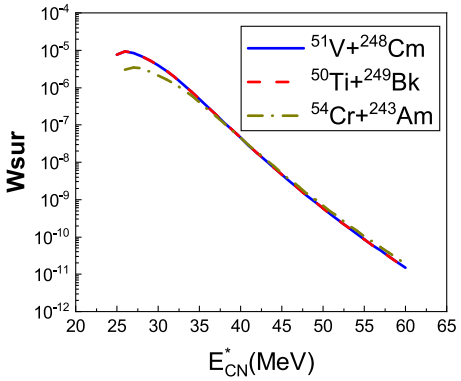

Fig. 3. (color online) Curves of survival probability of the compound nucleus formed in the three reactions as a function of the excitation energy.

cident energy for each reaction and reflect the maximum cross section value for synthesizing the target element under specific conditions. The maximum cross sections for the production of element 119 in the three reactions all occur on the curve corresponding to the evaporation of three neutrons. For the ^{50}Ti + ^{249}Bk reaction, the optimal incident energy is approximately 225.66 MeV, with a maximum cross section of 21.72 fb. For ^{51}V + ^{248}Cm , the optimal incident energy is approximately 229.86 MeV, with a maximum cross section of 12.7 fb. For ^{54}Cr + ^{243}Am, the optimal incident energy is approximately 241.65 MeV, with a maximum cross section of 2.29 fb.

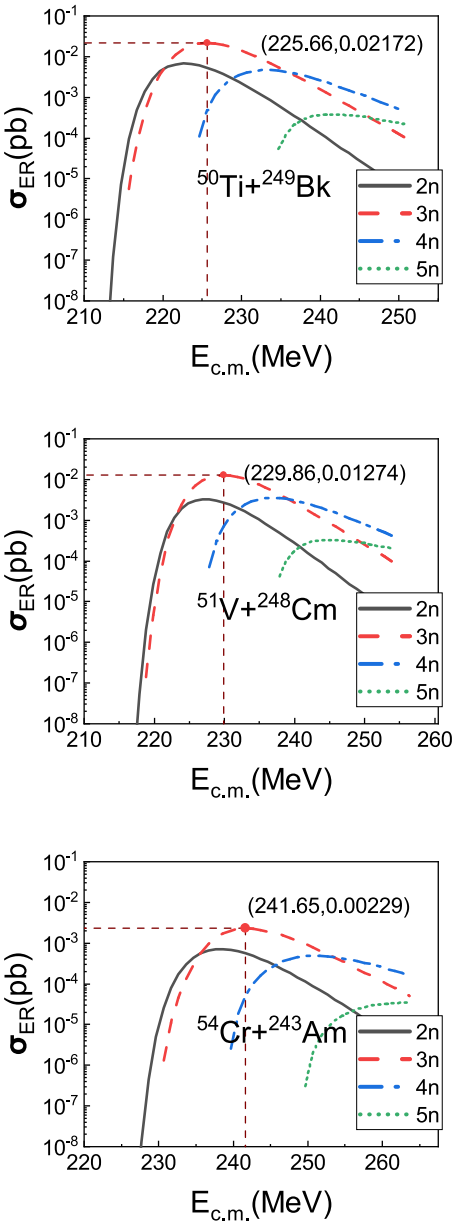

Fig. 4. (color online) Curves of the ERCS for the three reactions after evaporating 2–5 neutrons as a function of incident energy.

In Table 2, we present a comparison of the ERCS for the 3n and 4n channels and optimal incident energies for synthesizing element 119 obtained in this study using predictions from several studies [25, 50−57]. Among these, the first result from Ref. [57] is calculated using the DNS model, while the last two are computed using the weak-model-dependence method with different parameters. Our results corresponds with the ERCS values and optimal incident energies predicted in Refs. [51, 54, 57], further validating the accuracy and reliability of our calculations. The values of $E_{\rm c.m.}$ presented in the table correspond with the energies at which the maximum cross sections for the 3n and 4n channels were achieved, calculated using the various methods detailed in the aforementioned references. By comparing our data with results from other studies, we demonstrate strong consistency, further reinforcing the DNS model as a reliable tool for predicting the synthesis of superheavy elements. This study not only validates our findings but also provides valuable insights for future experimental efforts aimed at synthesizing element 119 under optimal conditions.

Table 2. Comparison of the theoretical predictions of the ERCS and optimal incident energies obtained in study with results presented in Refs. [25, 50−57].

Reaction	$E_{\rm c.m.}$/MeV	3*n*/fb	$E_{\rm c.m.}$/MeV	4*n*/fb	References
^{50}Ti + ^{249}Bk	225.66	21.72	233.66	4.68	This study
	224	11.9	236	64	[50]
	226	48.2	244	5.67	[51]
	225	29.8	233	35.6	[54]
	–	–	230	40	[52]
	–	–	230	18.7	[53]
	222.8	–	–	–	[57]
	224.9(224.3)	–	–	–	[57]
^{51}V + ^{248}Cm	229.86	12.7	236.86	3.57	This work
	225	6.6	232	12.3	[56]
	227	5.5	237	10.1	[50]
	228	2.9	236	5.9	[54]
	230	9.2	248	1.2	[51]
	232	19.5	245	99.6	[55]
	–	–	237	11.8	[52]
	233.0	–	–	–	[57]
	229.3(228.4)	–	–	–	[57]
^{54}Cr + ^{243}Am	241.65	2.29	251.65	0.49	This work
	236.65	25	–	–	[25]
	238.7	–	–	–	[57]
	241.4(241.6)	–	–	–	[57]

IV. SUMMARY

To determine the optimal reaction combinations for the synthesis of superheavy element $Z = 119$, we investigated the $^{51}V + ^{248}Cm$, $^{50}Ti + ^{249}Bk$, and $^{54}Cr + ^{243}Am$ reactions using the DNS model. Herein, we varied the incident energy from 210 MeV to 260 MeV and calculated the capture cross section, fusion probability, survival probability, and ERCS for each reaction. From this analysis, we identified the optimal incident energy and corresponding ERCS for each reaction. For the $^{50}Ti + ^{249}Bk$ reaction, the optimal incident energy is approximately 225.66 MeV, resulting in a maximum cross section of 21.72 fb. For the $^{51}V + ^{248}Cm$ reaction, the optimal energy is approximately 229.86 MeV, with a maximum cross section of 12.7 fb. For the $^{54}Cr + ^{243}Am$ reaction, the optimal energy is approximately 241.65 MeV, with a maximum cross section of 2.29 fb. These results provide a solid theoretical basis for further experimental studies, thereby facilitating the successful synthesis of element $Z = 119$.

V. ACKNOWLEDGMENTS

The authors would like to express their sincere gratitude to Prof. Zai-Guo Gan and Zhi-Yuan Zhang for their valuable discussions.

References

[1] K. Morita, Nucl. Phys. A **944**, 30 (2015)
[2] Yu. Ts. Oganessian, A. Sobiczewski, and G. M. Ter-Akopian, Phys. Scr. **92**(2), 023003 (2017)
[3] A. Sobiczewski, F..A. Gareev, and B. N. Kalinkin, Phys. Lett. **22**(4), 500 (1966)
[4] Yu. Ts. Oganessian, Rad. Phys. Chem. **61**(3), 259 (2001)
[5] C. W. Shen, Y. Abe, D. Boilley *et al.*, Int. J. Mod. Phys. E **17**(supp01), 66 (2008)
[6] S. Bjørnholm and W. J. Swiatecki, Nucl. Phys. A **391**(2), 471 (1982)
[7] W. J. Swiatecki, Prog. Part. and Nucl. Phys. **4**, 383 (1980)
[8] V. I. Zagrebaev and W. Greiner, Nucl. Phys. A **944**, 257 (2015)
[9] V. I. Zagrebaev, Phys. Rev. C **64**, 034606 (2001)
[10] V. Zagrebaev and W. Greiner, J. Phys. G: Nucl. Part. Phys. **34**(1), 1 (2007)
[11] V. L. Litnevsky, G. I. Kosenko, and F. A. Ivanyuk, Phys. Rev. C **93**, 064606 (2016)
[12] V. L. Litnevsky, V. V. Pashkevich, G. I. Kosenko *et al.*, Phys. Rev. C **89**, 034626 (2014)
[13] A. S. Umar, V. E. Oberacker, J. A. Maruhn *et al.*, Phys. Rev. C **81**, 064607 (2010)
[14] M. Tohyama and A. S. Umar, Phys. Rev. C **93**, 034607 (2016)
[15] G. G. Adamian, N. V. Antonenko, and W. Scheid, Phys. Rev. C **69**, 044601 (2004)
[16] Z. Q. Feng, G. M. Jin, J. Q. Li *et al.*, Phys. Rev. C **76**, 044606 (2007)
[17] N. Wang, J. q. Li, and E. g. Zhao, Phys. Rev. C **78**, 054607 (2008)
[18] Z. Q. Feng, G. M. Jin, and J. Q. Li, Phys. Rev. C **80**, 057601 (2009)
[19] M. h. Huang, Z. g. Gan, X. h. Zhou *et al.*, Phys. Rev. C **82**, 044614 (2010)
[20] M. h. Huang, Z. y. Zhang, Z. g. Gan *et al.*, Phys. Rev. C **84**, 064619 (2011)
[21] N. Wang, E. G. Zhao, W. Scheid *et al.*, Phys. Rev. C **85**, 041601 (2012)
[22] L. Zhu, Z. Q. Feng, C. Li *et al.*, Phys. Rev. C **90**, 014612 (2014)
[23] K. Rutz, M. Bender, T. Bürvenich *et al.*, Phys. Rev. C **56**(1), 238 (1997)
[24] W. Zhang, J. Meng, S. Q. Zhang *et al.*, Nucl. Phys. A **753**(1-2), 106 (2005)
[25] B. M. Kayumov, O. K. Ganiev, A. K. Nasirov *et al.*, Phys. Rev. C **105**, 014618 (2022)
[26] J. X. Li and H. F. Zhang, Phys. Rev. C **105**, 054606 (2022)
[27] F. Li, L. Zhu, Z. H. Wu *et al.*, Phys. Rev. C **98**, 014618 (2018)
[28] N. Wang, E. G. Zhao, and W. Scheid, Phys. Rev. C **89**, 037601 (2014)
[29] Yu. Ts. Oganessian, V. K. Utyonkov, Yu. V. Lobanov *et al.*, Phys. Rev. C **74**, 044602 (2006)
[30] N. V. Antonenko, E. A. Cherepanov, A. K. Nasirov *et al.*, Phys. Lett. B **319**(4), 425 (1993)
[31] W. f. Li, N. Wang, F. Jia *et al.*, J. Phys. G: Nucl. Part. Phys. **32**(8), 1143 (2006)
[32] N. V. Antonenko, E. A. Cherepanov, A. K. Nasirov *et al.*, Phys. Rev. C **51**, 2635 (1995)
[33] G. Giardina, S. Hofmann, A. I. Muminov *et al.*, Eur. Phys. J. A **8**, 205 (2000)
[34] A. S. Zubov, G. G. Adamian, N. V. Antonenko *et al.*, Phys. Rev. C **65**, 024308 (2002)
[35] D. L. Hill and J. A. Wheeler, Phys. Rev. **89**, 1102 (1953)
[36] Z. Q. Feng, G. M. Jin, F. Fu *et al.*, Nucl. Phys. A **771**, 50 (2006)
[37] P. Möller, A. J. Sierk, T. Ichikawa *et al.*, At. Data Nucl. Data Tables **109-110**, 1 (2016)
[38] W. D. Myers and W. J. Swiatecki, Nucl. Phys. **81**(1), 1 (1966)
[39] C. Y. Wong, Phys. Rev. Lett. **31**, 766 (1973)
[40] I. I. Gontchar, D. J. Hinde, M. Dasgupta *et al.*, Phys. Rev. C **69**, 024610 (2004)
[41] B. Wang, K. Wen, W. J. Zhao *et al.*, At. Data Nucl. Data Tables **114**, 281 (2017)
[42] M. H. Huang, Z. G. Gan, Z. Q. Feng *et al.*, Chin. Phys. Lett. **25**(4), 1243 (2008)
[43] W. Li, N. Wang, J. F. Li *et al.*, Eur. Lett. **64**(6), 750 (2003)
[44] S. Q. Guo, *Study of the fusion mechanism within the dinuclear system model*, PhD thesis, Lanzhou University, 2018, CNKI: CDMD: 1.1018.829018
[45] A. C. Merchant and W. Nörenberg, Z. Physik A. **308**, 315 (1982)
[46] J. Q. Li, Z. Q. Feng, Z. G. Gan *et al.*, Nucl. Phys. A **834**(1), 353c–356c (2010)
[47] N. Wang, J. S. Peng, E. G., Zhao *et al.*, Nucl. Phys. Rev. **30**(3), 294 (2013)
[48] C. Riedel, G. Wolschin, and W. Nörenberg, Z. Physik A.

290, 47 (1979)
[49] G. G. Adamian, N. V. Antonenko, W. Scheid *et al*., Nucl. Phys. A **627**(2), 361 (1997)
[50] L. Zhu, W. J. Xie, and F. S. Zhang, Phys. Rev. C **89**, 024615 (2014)
[51] X. J. Lv, Z. Y. Yue, W. J. Zhao *et al*., Phys. Rev. C **103**, 064616 (2021)
[52] G. G. Adamian, N. V. Antonenko, and H. Lenske, Nucl. Phys. A **970**, 22 (2018)
[53] G. G. Adamian, N. V. Antonenko, H. Lenske *et al*., Phys. Rev. C **101**, 034301 (2020)
[54] K. Siwek-Wilczyńska, T. Cap, and M. Kowal, Phys. Rev. C **99**, 054603 (2019)
[55] N. Ghahramany and A. Ansari, Eur. Phys. J. A **52**(9), 287 (2016)
[56] A. Nasirov and B. Kayumov, Phys. Rev. C **109**, 024613 (2024)
[57] L. Zhu, Phys. Rev. Res. **5**, L022030 (2023)